AIMS Materials Science, 4(1): 267-276.
DOI: 10.3934/matersci.2017.1.267
Received: 31 October 2016
Accepted: 24 January 2017
Published: 07 February 2017

http://www.aimspress.com/journal/Materials

Research article

ZnO nanonails for photocatalytic degradation of crystal violet dye under UV irradiation

Nirmalya Tripathy [1,*], Rafiq Ahmad [2], Jeong Eun Song [1], Hyun Park [1], and Gilson Khang [1,*]

[1] Department of BIN Fusion Technology, Department of Polymer-Nano Science & Technology, Polymer BIN Research Center, Chonbuk National University, 567 Baekje-daero, Deokjin-gu, Jeonju 561-756, Republic of Korea
[2] School of Semiconductor and Chemical Engineering, Nanomaterials Processing Research Center, Chonbuk National University, 567 Baekjedaero, Deokjin-gu, Jeonju 561-756, Republic of Korea

* **Correspondence:** nirmalya.t@gmail.com; gskhang@chonbuk.ac.kr; Tel: +82-63-270-2355; Fax: +82-63-270-2341.

Abstract: In this study, nanonails-like zinc oxide (ZnO) nanostructures were synthesized in large quantity by thermal evaporation technique and further characterized in detail using different techniques such as field emission scanning electron microscopy (FESEM), transmission electron microscopy (TEM), X-ray diffractometer (XRD), UV-visible spectroscopy, photoluminescence (PL) spectroscopy, and Raman spectroscopy. Morphological characterizations revealed that the as-synthesized nanostructures possess nail-like geometry, grown in large quantity. The XRD, UV-visible absorbance spectra, PL, and Raman spectra confirms good crystallinity and optical property of as-synthesized ZnO nanonails. The photocatalytic activities of designed nanostructures for crystal violet dye (CV-dye) degradation was evaluated under UV illumination and monitored by UV-vis spectroscopy at different time intervals until the dye was completely degraded to colorless end product. A fast decomposition was observed with ~95% degradation rate within the initial 70 min, which is attributed to high specific surface area (56.8 m^2/g), high crystallinity and better optical property of ZnO nanonails.

Keywords: ZnO; nanonails; thermal evaporation; crystal violet; photocatalytic activity

1. Introduction

Crystal violet dye (CV-dye), an important dye, is highly used to dye papers, ball-point pens, ink-jet printers and as colourizer of diverse products such as fertilizers, antifreezes, detergents, and leather. It is also used in biological science for staining purpose as well as in dye processing. This dye is mostly discharged as industrial waste into the environment, thereby possesses high threat to humans, other species and ecosystem as CV-dye can easily interact with negatively charged cells membrane surfaces, and can enter into cells and concentrate in cytoplasm [1,2]. The CV-dye is responsible for moderate eye irritation, causing painful sensitization to light. It can also cause permanent injury to the cornea and conjunctiva [3]. Inhalation of CV-dye may cause irritation to the respiratory tracks, vomiting, diarrhea, pain, headache, and dizziness. Long term exposure may cause damage to the mucous membrane and gastrointestinal tract [4]. Hence, its removal from industrial waste before releasing into the environment is a critical issue, which further stimulates the scientific community to develop a cheap and economical strategy for wastewater treatment.

Attempts have been made to use advanced oxidation process through heterogeneous photocatalysis under UV illumination on semiconductor surface. In this process, highly reactive free radicals were generated that leads to degradation/decomposition of organic chemicals present in the wastewater [5,6]. Among various semiconductor oxides, Zinc oxide (ZnO) is one of the highly appreciable materials for its versatile properties such as wide and direct fundamental band gap energy of 3.37 eV with large exciton binding energy (60 mV), piezoelectric, biocompatible nature, high mechanical and thermal stability. Previously, ZnO with diverse morphologies have been used in wide arena including chemical/biological sensors, solar cells, photovoltaic devices, photodynamic nanomaterial for drug delivery systems and as photocatalyst for treatment of organic and dye pollutants [7–20].

It has been reported that the photodegradation of organic matter in solution is catalyzed by photoexcitation of a semiconductor, which results in the generation of an electron-hole pair on the surface of photocatalyst [6]. The high oxidative potential of the hole in the catalyst permits direct oxidation of organic matter (OM) to reactive intermediates. Later, reactive hydroxyl radicals were formed by the decomposition of water and help in organic chemicals degradation [21,22,23]. Therefore, nanostructures having large specific surface area and high crystallinity with good surface permeability will provide feasible environment for organic pollutants transport and thus enhances catalytic behavior. In this context, nanonails morphology of ZnO offers both valuable properties, i.e., high surface area and excellent crystallinity. Additionally, spatial freedom in its orientation could provide better surface permeability for their potential applications in sensor fabrication and photocatalysis [24,25]. Recently, Daud et al. employed ZnO nanonails as photocatalytic hydrogen production and demonstrated that ZnO nanonails have higher densities of defects, which favor it for better contribution in photocatalytic activity [25]. Manthina and Agrios explored the synthesis of different nanostructures including ZnO fibers, nanorods, cauliflowers, nanorod balls, nanoforest, nanopencils, ellipsoids, and nanotubes using different additives and varying conditions [26]. They concluded that morphology change could change the properties of nanostructures. In this paper, we synthesized ZnO nanonails in large quantity by thermal evaporation technique and further exploited for the photocatalytic degradation of CV-dye under UV light irradiation. A fast decomposition was observed with a degradation rate of ~95% within the initial 70 min.

2. Materials and Method

2.1. Synthesis of ZnO Nanonails

To synthesize ZnO nanonails, high purity Zinc (Zn) powders (99.99%) were used as source material in a horizontal quartz tube furnace with halogen lamp heating system on non-catalytic Si (100) substrates and argon (Ar) gas supply. Where, ~0.2 g zinc powders were uniformly spread in an alumina boat and placed at the center of the furnace tube. A cleaned Si substrate was put in the quartz tube and the temperature was increased at a rate of 25 °C/min from room temperature to reaction temperature (600 °C), while flowing the Ar gas. The reaction was carried out for 90 min and then allowed to cool down at room temperature. Finally, grown ZnO nanonails on Si substrate was collected and characterized in detail in terms of their morphological, structural, compositional, optical, and photocatalytic properties. Additionally, to compare the photocatalytic efficiency, we also synthesized ZnO nanorods using our previous report [27]. In brief, 0.04 M of $Zn(NO_3)_2{\cdot}6H_2O$ and HMTA were dispersed in distilled water (50 mL); transferred into Pyrex glass bottle and heated at 85 °C for 4 h. The obtained product was washed to remove impurity and dried in air for further utilization as photocatalyst.

2.2. Characterization

The morphological characterizations were investigated by field emission scanning electron microscopy (FESEM, Hitachi S4700, equipped with energy dispersive spectroscopy (EDS)), and transmission electron microscopy (TEM, JEOL-JEM-2010 equipped with CCD camera). The crystallinity and crystal phase of the as-synthesized products were analyzed by X-ray diffraction (XRD, Rigaku) patterns with Cu-kα Radiation (λ = 1.54178 Å) in the range of 20–65^o scanned at 40 kV. The optical properties were characterized by room-temperature photoluminescence (PL) spectra and Raman-scattering measurements carried out at room temperature with the He-Cd (325 nm) laser line as excitation sources and with 514.5 nm line of an Ar^+ laser as the excitation source, respectively. The surface area of ZnO nanonails were measured by the Brunauer-Emmett-Teller (BET) using nitrogen adsorption-desorption isotherm analysis (ASAP 2010 analyzer at 77 K).

2.3. Photocatalytic Degradation of CV-dye

The photocatalytic degradation of CV-dye was performed using as-synthesized ZnO nanonails as photocatalyst under UV illumination for 0–70 min. The purchased CV-dye solution from Sigma Aldrich was prepared in 10 ppm solution and added with 0.1 g of as-synthesized ZnO nanostructures (nanonails and nanorods) into a conical flask under continuous stirring. Then, the suspension was stirred for 1 h in dark in order to stabilize the absorption of CV-dye over the photocatalyst surface. Afterwards, the photoreaction vessel was exposed to UV light under ambient conditions while stirring. At specific time intervals, the photoreacted suspension (2 mL) was taken out in every 10 min and centrifuged at 5000 rpm to separate the catalyst (ZnO nanostructures). The change in the absorption peak maximum in the UV-visible spectra of CV-dye was monitored using UV-visible spectrophotometer (2550-Shimadzu, Japan). The percentage of degradation of dye was estimated

using the following equation:

$$\text{Degradation rate (\%)} = (C_0 - C)/C_0 \times 100 \quad (1)$$

Where, C_0 and C are the concentrations of CV-dye at initial and at a particular time in the reactor, respectively.

3. Results and Discussion

The as-synthesized ZnO products has morphologically characterized by FESEM. The low-resolution FESEM image in Figure 1(a) shows that the ZnO nanonails were grown in large quantity on the Si substrate and consists of nail-like geometry with hexagonal tip. Interestingly, it seems that several nanonails were arranged forming a trunk-like structure (Figure 1(b) and (c)). The typical EDS spectrum of the nanonails in Figure 1(d) shows that the nanonails are composed of Zn and O elements only which also confirm the successful formation of ZnO nanostructures. Figure 2 shows the low- (a) and high-resolution (b) TEM image of as-grown ZnO nanonails. From the low-resolution TEM image of single ZnO nanonail, the engineered nanostructure possesses smooth and clean surface demonstrating that no nanoclusters or tiny nanocrystals are formed at the top of nanonails. TEM image also reveals the full consistency with the FESEM observations in terms of morphology and dimensionality. The TEM image clearly shows that the nanonails structure possesses a hexagonal tip on one side of the trunk. The high-resolution TEM image (Figure 2(b)), shows the perfect lattice structure with a lattice distance between two lattice fringes as ~0.52 nm, which corresponds to the d-spacing of [0001] crystal plans, consistent with the bulk wurtzite crystal of ZnO. Additionally, the SEAD patterns are also fully consistent with the HRTEM observations (inset in Figure 2(a)).

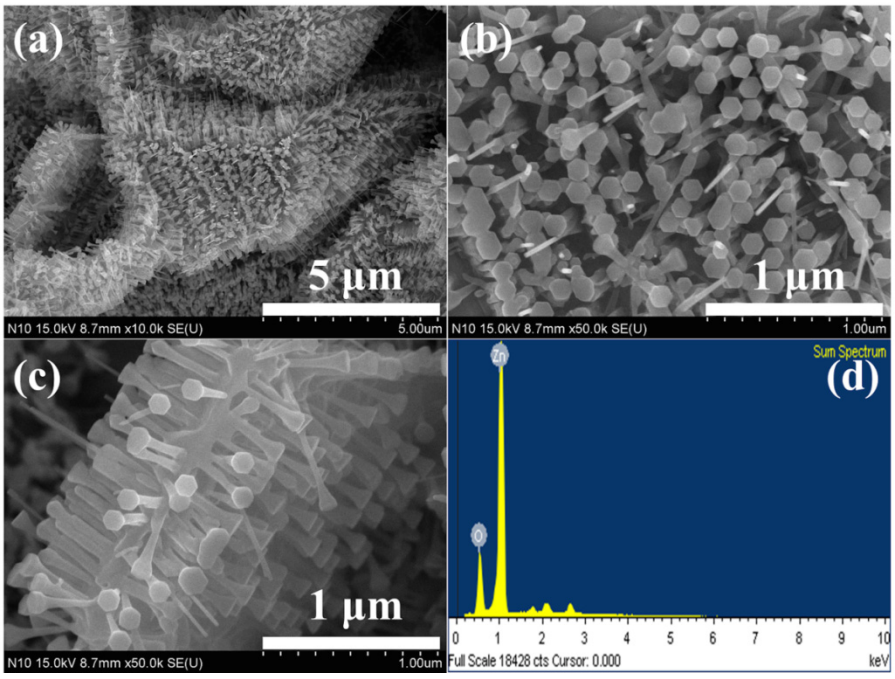

Figure 1. Typical low- (a) and high-magnification (b and c) FESEM images with EDS spectrum (d) of as-synthesized ZnO nanonails.

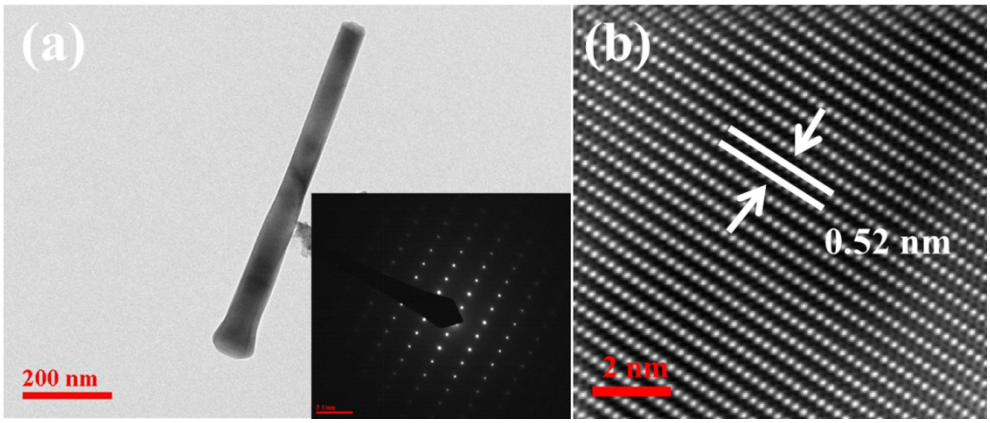

Figure 2. (a) Low-resolution TEM image of single ZnO nanonail along with SAED pattern in the inset, and (b) high-resolution TEM image indicating [0001] growth direction with a distance between two lattice fringes of ~0.52 nm.

Further, the crystallinity, optical property, and structural disorders and the defects of the as-synthesized ZnO nanonails were examined by XRD, room-temperature PL spectrum, and Raman scattering spectroscopy, respectively (Figure 3).

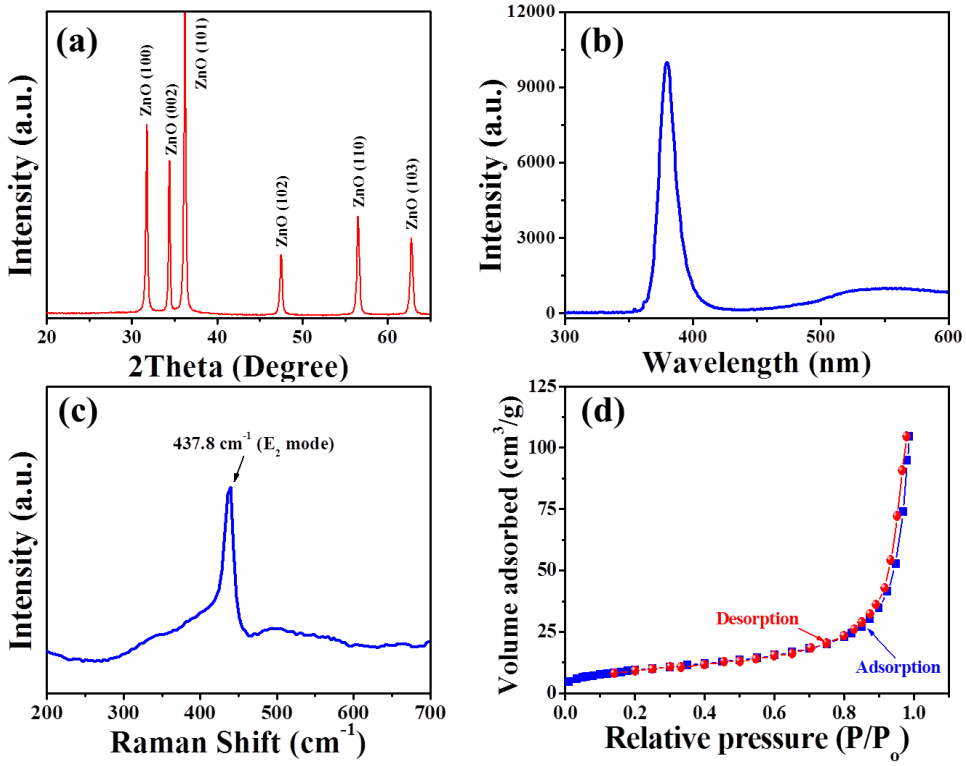

Figure 3. (a) XRD pattern, (b) room-temperature PL spectrum, (c) typical Raman spectra, and (d) Nitrogen adsorption-desorption isotherm of as-grown ZnO nanonails.

XRD spectrum of the nanostructures shows that all the diffraction peaks were indexed to the wurtzite structured hexagonal phase of single crystalline bulk ZnO with lattice constant of a =

3.249 Å and c = 5.206 Å (JCPDS card No. 35-1451). The typical PL spectrum shows a high intensity, sharp and strong peak at 379 nm in the UV region and further confirms the highly crystalline nature of ZnO with the wurtzite hexagonal phases. Additionally, in Figure 3(c) Raman scattering spectra shows a clear and dominant peak at 437.8 cm^{-1}, which corresponds to the Raman-active optical-phonon E_2 mode of wurtzite ZnO [28,29]. Importantly, there was no peak for E_{1L} mode that is associated with interstitial zinc, oxygen vacancies, and their complexes. Therefore, the synthesized ZnO nanonails offer high quality crystals without oxygen vacancies that could lead to a high photocatalytic activity towards dye degradation. Additionally, surface area of nanostructure materials is another important factor for better photocatalytic activity. We evaluated the surface area of as-synthesized ZnO nanonails using nitrogen adsorption-desorption isotherm, as shown in Figure 3(d). The ZnO nanonails offered high BET specific surface area, i.e., 56.8 m^2/g, which is found to be better than other ZnO nanostructures including nanoparticles, nanodisks, and nanomultipods, nanorods, and nanoplates [30,31,32]. Thus ZnO nanonails with larger surface area may provide active sites for photocatalytic degradation of dyes.

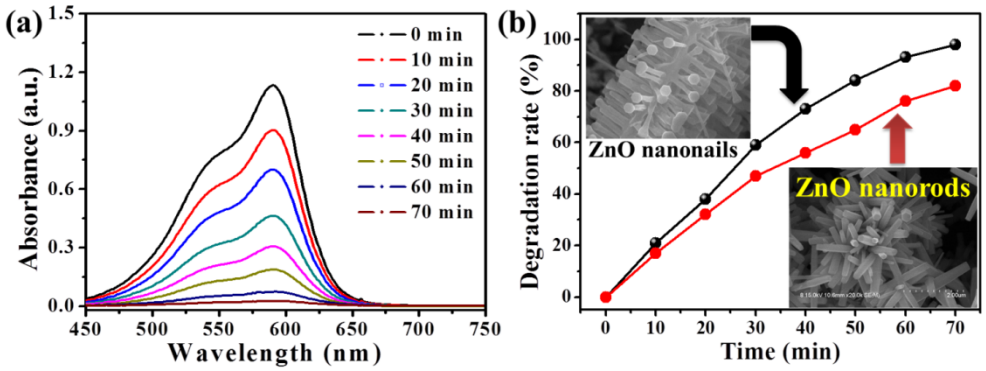

Figure 4. (a) UV-visible absorbance spectra of decomposed CV-dye solution over ZnO nanonails under UV light illumination and (b) Calibration curve of the degradation rate (%) versus time interval for ZnO nanonails and nanorods. Inset of b shows FESEM images of ZnO nanonails and nanorods.

The degradation of CV-dye was examined by UV-visible absorbance spectra over the surface of ZnO nanonails photocatalyst under UV illumination (Figure 4(a)). The spectra show that with increasing UV exposure time (0–70 min), the absorbance of CV-dye decreases indicating reduction/decomposition of CV-dye over ZnO nanonails. After 70 min of exposure time, the absorbance of CV-dye decreased to ~95%, suggesting rapid degradation of dye. Figure 4(b) shows the calibration curve of the rate of CV-dye degradation (%) versus time interval. During initial UV exposure time, a sharp increase in the dye degradation percentage is observed, which is due to the high adsorption of CV-dye on the surface of ZnO nanonails. However, a fast degradation rate of ~95% obtained within a short exposure time of 70 min. From the pie chart (inset of Figure 4(b)), the major CV-dye degradation is observed during the first 40 min over the ZnO nanonails surface. Recently, the CV-dye degradation ability of different ZnO structures was also prominent such as dumbbell-shaped ZnO microcrystal [33] by 68.0% within 75 min; hollow prism like ZnO nanostructures [34] by 91% within 75 min; coralline-like ZnO nanostructures [34] by 55% within 75 min and in ZnO hollow spheres [34] 79.5% degradation was achieved within 75 min under UV irradiation. Compared with

the above studies, ZnO nanonails shows enhanced photocatalytic degradation efficiency of CV-dye, which is attributed to the high crystallinity and better optical property of the as-grown ZnO nanonails. Moreover, in order to justify the potency of ZnO nanonails for photocatalytic activity, we have presented a comparison with ZnO nanorods and shown in Figure 4(b). Herein, we have synthesized ZnO nanorods using our previously published protocol followed by photocatalytic experiments. Compared to the ZnO nanonails efficiency of ~95% degradation rate, the ZnO nanorods demonstrated a lower performance (~82%) with same exposure time of 70 min (Figure 4(b)). This may be attributed to the larger size of ZnO nanorods providing lesser surface area for photocatalytic activity [32].

The fast degradation of CV-dye under UV light illumination (Figure 5) was explained by the photogeneration of electron-hole (e^--h^+) pairs between the conduction (CB) and valence bands (VB) due to excitation of ZnO [6,35,36]. Where, the photogenerated e^- in CB migrates to the surface; scavenged by the ubiquitous O_2 to produce super oxide anion O_2^- and simultaneous protonation produces HOO· radicals. While, h^+ in VB moves to the backside of ZnO nanonails surface and reacts with either H_2O or OH^- to yield an active species such as OH·. The generation of active radicals (O_2^-, $O_2\cdot^-$, HOO·/·OH) assists the mineralization of intermediates formed during catalytic degradation into the final, less harmful mineralized end products. Thus, fast photocatalytic degradation of CV-dye under UV illumination is assigned to high crystallinity and better optical features of ZnO nanonails that substantially increases the reactive species over catalysts surface.

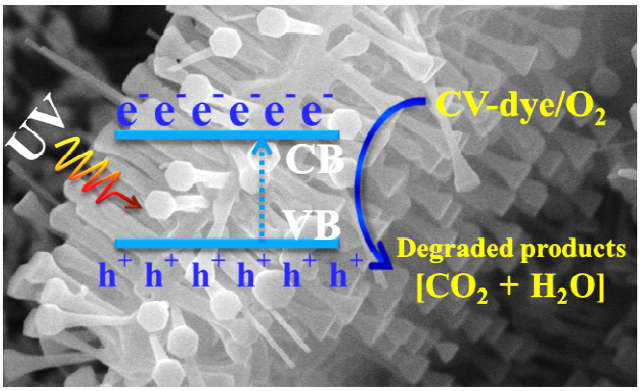

Figure 5. Schematic illustrations for photocatalytic degradation of CV-dye over the surface of ZnO nanonails.

4. Conclusion

The ZnO nanonails photocatalyst were successfully synthesized by thermal evaporation technique in large quantity and possesses high crystallinity and better optical characteristics. An enhanced photocatalytic feature of ZnO nanonails photocatalyst was studied for the degradation of CV-dye. After 70 min of photocatalytic degradation, the CV-dye degradation rate was observed to be ~95% for ZnO nanonails, which is more effective compared to ZnO nanorods (~82% degradation rate). Overall, the above results indicate that the as-prepared ZnO nanonails can be envisioned as a potential photocatalyst for efficient, rapid degradation of CV-dye into less harmful organics/minerals.

Acknowledgments

This work was supported by WCU program (R31-2009), Brain Korea 21 PLUS Project, NRF-2012M3A9C6050204, and Bio-industry Technology Development Program (KMFAFF, 112007-05-2-SB010).

Conflict of Interest

The authors declare no conflicts of interest regarding this paper.

References

1. Li S (2010) Removal of crystal violet from aqueous solution by sorption into semi-interpenetrated networks hydrogels constituted of poly(acrylic acid-acrylamide-methacrylate) and amylose. *Bioresource Technol* 101: 2197–2202.
2. Singh KP, Gupta S, Singh AK, et al. (2011) Optimizing adsorption of crystal violet dye from water by magnetic nanocomposite using response surface modeling approach. *J Hazard Mater* 186: 1462–1473.
3. Jone JJ, Falkinham JO (2003) Decolorization of malachite green and crystal violet by waterborne pathogenic mycobacteria. *Antimicrob Agents Ch* 47: 2323–2326.
4. Ghosh D, Bhattacharyya KG (2002) Adsorption of methylene blue on kaolinite. *Appl Clay Sci* 20: 295–300.
5. Chen CY, Kuo JT, Yang HA, et al. (2013) A coupled biological and photocatalysis pretreatment system for the removal of crystal violet from wastewater. *Chemosphere* 92: 695–701.
6. Khataee AR, Zarei M (2011) Photocatalysis of a dye solution using immobilized ZnO nanoparticles combined with photoelectrochemical process. *Desalination* 273: 453–460.
7. Yao H, Li F, Lutkenhaus J, et al. (2016) High-performance photocatalyst based on nanosized ZnO-reduced graphene oxide hybrid for removal of Rhodamine B under visible light irradiation. *AIMS Mater Sci* 3: 1410–1425.
8. Tripathy N, Ahmad R, Kuk H, et al. (2016) Mesoporous ZnO nanoclusters as an ultra-active photocatalyst. *Ceram Int* 42: 9519–9526.
9. Hahn YB, Ahmad R, Tripathy N (2012) Chemical and biological sensors based on metal oxide nanostructures. *Chem Commun* 48: 10369–10385.
10. Ahmad R, Tripathy N, Jung DUJ, et al. (2014) Highly sensitive hydrazine chemical sensor based on ZnO nanorods field-effect transistor. *Chem Commun* 40: 1890–1893.
11. Tripathy N, Ahmad R, Jeong HS, et al. (2012) Time-dependent control of hole-opening degree of porous ZnO hollow microspheres. *Inorg Chem* 51: 1104–1110.
12. Ahmad R, Tripathy N, Hahn YB (2013) High-performance cholesterol sensor based on the solution-gated field effect transistor fabricated with ZnO nanorods. *Biosens Bioelectron* 45: 281–286.
13. Tripathy N, Ahmad R, Kuk H, et al. (2016) Rapid methyl orange degradation using porous ZnO spheres photocatalyst. *J Photoch Photobio B* 161: 312–317.

14. Ahmad R, Tripathy N, Park JH, et al. (2015) A comprehensive biosensor integrated with a ZnO nanorod FET array for selective detection of glucose, cholesterol and urea. *Chem Commun* 51: 11968–11971.
15. Tripathy N, Ahmad R, Bang SH, et al. (2016) Outstanding antibiofilm features of quanta-CuO film on glass surface. *ACS Appl Mater Inter* 8: 15128–15137.
16. Ramakrishnan R, Devaki SJ, Aashish A, et al. (2016) Nanostructured semiconducting PEDOT-TiO_2/ZnO hybrid composites for nanodevice applications. *J Phys Chem C* 120: 4199–4210.
17. Khan R, Hassan MS, Cho HS, et al. (2014) Facile low-temperature synthesis of ZnO nanopyramid and its application to photocatalytic degradation of methyl orange dye under UV irradiation. *Mater Lett* 133: 224–227.
18. Tripathy N, Ahmad R, Bang SH, et al. (2014) Tailored lysozyme-ZnO nanoparticle conjugates as nanoantibiotics. *Chem Commun* 50: 9298–9301.
19. Zhang X, Qin J, Xue Y, et al. (2013) Effect of aspect ratio and surface defects on the photocatalytic activity of ZnO nanorods. *Sci Rep* 4: 4596.
20. Tripathy N, Ahmad R, Ko HA, et al. (2015) Enhanced anticancer potency using an acid-responsive ZnO-incorporated liposomal drug-delivery system. *Nanoscale* 7: 4088–4096.
21. Daneshvar N, Salari D, Khataee AR (2004) Photocatalytic degradation of azo dye acid red 14 in water on ZnO as an alternative catalyst to TiO_2. *J Photoch Photobio A* 162: 317–322.
22. Bachman J, Patterson HH (1999) Photodecomposition of the carbamate pesticide carbofuran: Kinetics and the influence of dissolved organic matter. *Environ Sci Technol* 33: 874–881.
23. Daneshvar N, Rasoulifard MH, Khataee AR, et al. (2007) Removal of C.I. Acid Orange 7 from aqueous solution by UV irradiation in the presence of ZnO nanopowder. *J Hazard Mater* 143: 95–101.
24. Umar A, Rahman MM, Kim SH, et al. (2008) Zinc oxide nanonail based chemical sensor for hydrazine detection. *Chem Commun* 166–168.
25. Daud SNHM, Haw C, Chiu W, et al. (2016) ZnO nanonails: Organometallic synthesis, self-assembly and enhanced hydrogen gas production. *Mat Sci Semicon Proc* 56: 228–237.
26. Manthina V, Agrios AG (2016) Single-pot ZnO nanostructure synthesis by chemical bath deposition and their applications. *Nano-Struct Nano-Object* 7: 1–11.
27. Ahmad R, Tripathy N, Khan MY, et al. (2016) Ammonium ion detection in solution using vertically grown ZnO nanorod based field-effect transistor. *RSC Adv* 6: 54836–54840.
28. Li L, Yang H, Qi G, et al. (2008) Synthesis and photoluminescence of hollow microspheres constructed with ZnO nanorods by H_2 bubble templates. *Chem Phys Lett* 455: 93–97.
29. Xu XL, Lau SP, Chen JS, et al. (2001) Polycrystalline ZnO thin films on Si (100) deposited by filtered cathodic vacuum arc. *J Cryst Growth* 223: 201–205.
30. Lv Y, Yu L, Huang H, et al. (2012) Application of the soluble salt-assisted route to scalable synthesis of ZnO nanopowder with repeated photocatalytic activity. *Nanotechnology* 23: 065402.
31. Zhang Y, Wu H, Huang X, et al. (2011) Effect of substrate (ZnO) morphology on enzyme immobilization and its catalytic activity. *Nanoscale Res Lett* 6: 450–456.
32. Kaneti YV, Zhang Z, Yue J, et al. (2014) Crystal plane-dependent gas-sensing properties of zinc oxide nanostructures: experimental and theoretical studies. *Phys Chem Chem Phys* 16: 11471–11480.

33. Sun JH, Dong SY, Wang YK, et al. (2009) Preparation and photocatalytic property of a novel dumbbell-shaped ZnO microcrystal photocatalyst. *J Hazard Mater* 172: 1520–1526.
34. Kowsari E (2011) Sonochemically assisted synthesis and application of hollow spheres, hollow prism, and coralline-like ZnO nanophotocatalyst. *J Nanopart Res* 8: 3363–3376.
35. Lv J, Gong W, Huang K, et al. (2011) Effect of annealing temperature on photocatalytic activity of ZnO thin films prepared by sol-gel method. *Superlattice Microst* 50: 98–106.
36. Khan MM, Lee J, Cho MH (2014) Au@TiO_2 nanocomposites for the catalytic degradation of methyl orange and methylene blue: An electron relay effect. *J Ind Eng Chem* 20: 1584–1590.

AIMS Press